• Basic Research •

Nuclear translocation of pyruvate kinase M2 drives high glucose-induced angiogenesis in retinal endothelial cells *via* the HIF-1α axis

Tian-Yi Liu[1], Ya-Jing Tian[1], Peng-Zhou Kuai[1], Yi-Sheng Luo[1], Cheng-Wei Duan[2], Tian-Peng Chen[2], Xiao-Le Wang[1], Dong-Mei Zhang[2], Xin Cao[1]

[1]Department of Ophthalmology, Affiliated Nantong Clinical College of Nantong University, Nantong First People's Hospital, Nantong 226001, Jiangsu Province, China
[2]Clinical Medical Research Center, Nantong First People's Hospital, Nantong 226001, Jiangsu Province, China
Co-first Authors: Tian-Yi Liu and Ya-Jing Tian
Correspondence to: Xin Cao. Department of Ophthalmology, Affiliated Nantong Clinical College of Nantong University, Nantong First People's Hospital, Nantong 226001, Jiangsu Province, China. caoxin512@163.com
Received: 2025-10-22 Accepted: 2026-01-28

Abstract

● **AIM:** To investigate the role of pyruvate kinase M2 (PKM2) in high glucose (HG)-stimulated retinal endothelial cells and its underlying molecular mechanisms and signaling pathways in retinal angiogenesis.

● **METHODS:** Human retinal microvascular endothelial cells (HRMECs) were cultured and divided into the following groups: normal glucose (NG, 5.5 mmol/L), HG (30 mmol/L), HG with PKM2 knockdown (HG+shPKM2), and HG treated with the pharmacological activator TEPP-46 (HG+TEPP-46). Cellular viability, proliferation, migration, and tube-forming ability were assessed using CCK-8, EdU, wound healing/Transwell, and Matrigel assays, respectively. The expression levels of PKM2, phosphorylated PKM2 (p-PKM2, Y105), hypoxia-inducible factor-1α (HIF-1α), and vascular endothelial growth factor A (VEGFA) were detected by Western blotting. The oligomerization status of PKM2 was analyzed *via* native gel electrophoresis. The subcellular localization of PKM2 was examined by immunofluorescence and nuclear-cytoplasmic fractionation.

● **RESULTS:** Under HG stimulation, the expression level of PKM2 was significantly increased (P<0.05). Knockdown of PKM2 was found to markedly suppress cell viability, proliferation, migration, and tube formation in HRMECs (P<0.05). Mechanistic studies revealed that phosphorylation of PKM2 at the Y105 site was promoted by HG treatment, which induced its dissociation from a tetramer to a dimer, thereby driving its nuclear translocation. Upon entering the nucleus, PKM2 was shown to exert critical non-metabolic functions; it was physically bound to HIF-1α and acted as its co-activator, leading to significant upregulation of VEGFA expression (P<0.05). In contrast, the PKM2 activator TEPP-46 effectively prevented dimerization and nuclear translocation of PKM2 by promoting its tetramerization. Consequently, the PKM2/HIF-1α axis-mediated upregulation of VEGFA was blocked, ultimately resulting in the reversal of HG-induced angiogenesis.

● **CONCLUSION:** HG influences retinal endothelial cell function by inducing PKM2 phosphorylation, dimerization, and nuclear translocation. The shift in PKM2 phosphorylation and oligomerization status represents a key mechanism through which TEPP-46 reverses HG-induced angiogenesis.

● **KEYWORDS:** retinal endothelial cells; glucose angiogenesis; nuclear translocation; pyruvate kinase M2; hypoxia-inducible factor-1α

DOI:10.18240/ijo.2026.05.03

Citation: Liu TY, Tian YJ, Kuai PZ, Luo YS, Duan CW, Chen TP, Wang XL, Zhang DM, Cao X. Nuclear translocation of pyruvate kinase M2 drives high glucose-induced angiogenesis in retinal endothelial cells *via* the HIF-1α axis. *Int J Ophthalmol* 2026;19(5):858-868

INTRODUCTION

Diabetic retinopathy (DR) is defined by characteristic retinal microvascular lesions arising from the metabolic disturbances of diabetes[1-3]. Driven by sustained hyperglycemia and a chronic inflammatory response, the retinal tissue undergoes a series of pathological alterations, including endothelial cell apoptosis, blood-retinal barrier (BRB) disruption, and increased vascular permeability. These changes further exacerbate retinal ischemia and hypoxia, ultimately leading to the formation of aberrant new blood vessels[4-5]. This pathological angiogenesis—a multi-step

process involving endothelial proliferation, migration, and tube formation—is a hallmark of proliferative DR (PDR) and a primary cause of vision loss[6-8]. Although current clinical interventions—such as laser photocoagulation, intravitreal anti-vascular endothelial growth factor (VEGF) injections, and vitreoretinal surgery—primarily target advanced stages of the disease, their therapeutic efficacy remains limited[9]. Therefore, elucidating the molecular mechanisms of angiogenesis in DR is of significant scientific and clinical importance for the development of novel treatment strategies.

Pyruvate kinase M2 (PKM2), a key catalytic enzyme in the glycolytic pathway, not only regulates intracellular glycolytic flux but also exhibits non-glycolytic functions[10-12]. Studies have shown that PKM2 participates in angiogenesis through various mechanisms, including modulation of ATP production, influence on endothelial tight junctions, and regulation of mitochondrial dynamics[13-15]. PKM2 exhibits conformation-dependent multifunctionality: the tetrameric form possesses high pyruvate kinase activity and primarily regulates glycolysis, whereas the dimeric form displays non-canonical protein kinase activity and can translocate into the nucleus to participate in gene expression regulation[16-18]. Furthermore, clinical data indicate elevated PKM2 levels in the plasma of diabetic patients, while the expression of the highly active tetrameric form is downregulated in models of diabetic nephropathy, suggesting a close association between its conformational changes and the progression of metabolic diseases[19]. These findings collectively support the potential role of PKM2 as a key metabolic-transcriptional integrator in angiogenesis.

Emerging evidence indicates that PKM2 and hypoxia-inducible factor-1α (HIF-1α) form a critical functional axis. PKM2 acts as a transcriptional coactivator of HIF-1α, enhancing its regulatory capacity for downstream target genes—including vascular endothelial growth factor A (VEGFA)—thereby establishing a positive feedback loop that promotes both angiogenesis and glycolysis[14,20]. Under high glucose (HG) and hypoxic conditions, PKM2 undergoes dimerization and nuclear translocation, PKM2 interacts with HIF-1α to regulate VEGFA secretion, thereby promoting tumor angiogenesis[21]. In models of diabetic nephropathy, the PKM2-specific activator TEPP-46 confers renal protection against inflammation by inhibiting PKM2 phosphorylation and promoting its active conformational state[19]. However, the role of PKM2 in HG-induced angiogenesis in human retinal microvascular endothelial cells (HRMECs) within the context of DR remains unclear. Therefore, our study intends to investigate the influence of PKM2 on angiogenesis in HRMECs under HG conditions and to explore its underlying molecular mechanisms.

MATERIALS AND METHODS

Cell Culture and Treatment The HRMEC line was obtained commercially from the BeNa Culture Collection (Beijing, China) and used without further authentication[22]. Cells were maintained in complete low-glucose DMEM (Hyclone) supplemented with 10% fetal bovine serum (FBS; Lonsa) and 1% penicillin-streptomycin (Beyotime, China) at 37°C with 5% CO_2. All experiments were conducted using HRMECs between passages 3 and 8 to ensure phenotypic stability. Experimental groups were treated for 48h with normal glucose (NG, 5.5 mmol/L D-glucose), HG (30 mmol/L D-glucose), high mannitol (HM, 25 mmol/L mannitol+5 mmol/L D-glucose) or HG co-administered with the PKM2 activator TEPP-46 (10 μmol/L)[19]. All experiments were conducted in accordance with standard institutional research practices.

DNA Construct and Cell Infection To achieve stable knockdown of PKM2, a green fluorescent protein (GFP) -tagged lentiviral vector system was employed. The non-targeting control shRNA (shNC) plasmid and PKM2-specific shRNA plasmid were purchased from Genepharma (Shanghai, China). The targeting sequence for human PKM2 shRNA was: 5'-CTACCACTTGCAATTATTTGA-3'[23].

Lentiviruses were generated by co-transfecting HEK293T cells with either LV3-shNC or LV3-PKM2 shRNA plasmid, together with the PSPAX2 packaging and PMD2.G envelope plasmids, using standard protocols. The viral supernatant was harvested at 48h post-transfection, subsequently filtered through a 0.45-μm membrane, and aliquoted for storage at -80°C. For viral infection, HRMECs were subjected to viral particles in the presence of 10 μmol/L Forskolin for 6-12h, followed by a 48-hour culture in fresh low-glucose Dulbecco's Modified Eagle Medium (DMEM). Transduction efficiency was monitored *via* GFP fluorescence, and PKM2 knockdown was validated using immunofluorescence microscopy, quantitative real-time polymerase chain reaction (qRT-PCR) and Western blotting (WB)[24]. Prior to experimentation, the transduced cells were subjected to 48-hour treatment with NG or HG.

CCK-8 Proliferation Assay Cell viability was assessed using the Cell Counting Kit-8 (CCK-8; PF00004, Proteintech, China) following the manufacturer's protocol. Briefly, HRMECs were spread in 96-well plates at a density of 3×10^3 per well and maintained at 37°C with 5% CO_2. After 24, 48, or 72h of culture, 10 μL of CCK-8 solution was added to each well, and the plates were incubated for an additional 1h. Absorbance was assessed at 450 nm employing a BIOTEK microplate reader (USA). Cell viability was then calculated as a percentage with reference to the control group.

Scratch-wound Assay We assessed cell migration with a scratch-wound assay. HRMECs were seeded in 6-well plates and allowed to reach full confluence over a 16-hour period

Table 1 Primer sequences used for qPCR assays

Gene	Forward (5′-3′)	Reverse (5′-3′)
PKM2	TGAGGCAGAGGCTGCCATCTACCACTT	TGCCAGACTTGGTGAGGACGATTATGGC
HIF-1α	CTTGGACGCTCTGCCTATGA	AGGTTGCGGGGGTTGTAGAT
VEGFA	CAGAGCGGAGAAAGCATTTG	TGGTTCCCGAAACCCTGAGG
GAPDH	TCAAGAAGGTGGTGAAGCAG	TCGCTGTTGAAGTCAGAGGA

qPCR: Quantitative polymerase chain reaction; *PKM2*: Pyruvate kinase M2; *HIF-1α*: Hypoxia-inducible factor-1α; *VEGFA*: Vascular endothelial growth factor A; *GAPDH*: Glyceraldehyde-3-phosphate dehydrogenase.

prior to wounding. Then, scrape the surfaces of the dishes with 100 μL pipette tip. After washing, the cells were returned to the incubator, and wound closure was monitored at 0, 12, and 24h post-scratching under a TS2 biomicroscope. The migration ability was determined by measuring the changes in wound width over time.

Transwell Assay The Transwell assay was conducted following a previously described method[25], with minor modifications. Briefly, cell invasion was assessed using 24-well Transwell chambers with 8-μm pore polyethylene terephthalate (PET) membranes (353097, Corning, USA). Add 300 μL of serum-free medium containing 5×10^4 pretreated HRMECs to the upper chamber. The chamber was placed into a 24 well plate prefilled with 600 μL of complete medium supplemented with 10% FBS. Following a 24-hour incubation, after removing non-migrated cells from the upper surface with a cotton swab, the adherent cells on the lower membrane were stained with 0.1% crystal violet and counted using a biomicroscope (TS2, Nikon, Germany).

Tube Formation Assay Angiogenic capacity was evaluated using a tube formation assay based on a reported method[25], with minor modifications. Following seeding on Matrigel-coated 96-well plates (2×10^4 cells/well), HRMECs were incubated for 4h. Tube formation was then documented at 40× magnification, and network quantification was performed using ImageJ software.

Western Blotting Analysis HRMECs were lysed with Tris-buffered saline (TBS) buffer containing 1% Triton X-100, supplemented with protease and phosphatase inhibitors, and total protein was extracted. After determining protein concentration using a bicinchoninic acid (BCA) kit (Thermo Fisher Scientific, USA), 20 μg of each protein sample was resolved by sodium dodecyl sulfate-polyacrylamide gel electrophoresis (SDS-PAGE) and transferred to polyvinylidene fluoride (PVDF) membranes. Following blockage in 5% skim milk for 2h at room temperature, the membranes were incubated overnight at 4°C with specific primary antibodies: anti-VEGFA (66828-1-Ig, proteintech, China), anti-HIF-1α (20960-1-AP, proteintech, China), anti-vascular endothelial growth factor receptor 2 (VEGFR2; 26415-1-AP, proteintech, China), anti-PKM2 (D78A4, Cell Signaling Technology, MA, USA), anti-p-PKM2 at tyrosine 105 (Y105; 3827S, Cell Signaling Technology, MA, USA), anti-glyceraldehyde-3-phosphate dehydrogenase (GAPDH; 60004-1-Ig, proteintech, China) and anti-α-tubulin (66031-1-Ig, proteintech, China). To detect specific immunoreactivity, the membranes were subjected to a 2-hour incubation with corresponding secondary antibodies at room temperature after thorough washes. Protein bands were visualized by chemiluminescence [enhanced chemiluminescence (ECL) kit, PK10003, Proteintech, China] and quantified by densitometry using Image J software.

Quantitative Real-Time PCR After the indicated treatments, Trizol reagent was added, total RNA was isolated using the chloroform method, and the purity and concentration of the RNA were assessed by measuring its absorbance at 260/280 nm. Subsequently, 1 μg of RNA was reverse-transcribed into cDNA using the PrimeScript RT Master Mix (Takara, China) according to the manufacturer's protocol. The cDNA products were then stored at -20°C for later use. qRT-PCR was performed with the 2× ChamQ Universal SYBR qPCR Master Mix (Vazyme, China) to evaluate gene expression levels. VEGFA primers target a sequence common to all major splice variants, detecting total VEGFA mRNA. The $2^{-\Delta\Delta Ct}$ method was applied to calculate relative mRNA expression levels, with GAPDH serving as the endogenous reference gene for data normalization (Table 1).

Immunofluorescence HRMECs were seeded onto coverslips in a 24-well plate for 48h. Following attachment, cells were briefly rinsed, fixed in pre-chilled 4% paraformaldehyde at -20°C for 20min, and permeabilized with 0.3% Triton X-100. Subsequently, nonspecific sites were blocked with a buffer containing 10% FBS for 2h at room temperature. We incubated the cells overnight at 4°C with primary antibodies for PKM2 (1:200) and HIF-1α (1:200), using a blocking buffer consisting of 1% BSA, 1% FBS, and 0.3% Triton X-100. After rewarming and washing, samples were treated with fluorophore-conjugated secondary antibodies (1:1000; 1.5h, 4°C). Subsequently, nuclei were labeled with 4',6-diamidion-2-phenylindole (DAPI) in the dark, and coverslips were prepared for final imaging using a fluorescence microscope (ECLIPSE Ni-E, Nikon, Germany).

Nuclear and Cytoplasmic Fraction The nuclear and cytoplasmic fractionation assay was performed using a cytoplasmic extraction reagents kit (78833, Thermo Fisher

Scientific, USA) according to the manufacturer's instructions. Briefly, pretreated HRMECs were harvested, counted, and 2×10^6 cells were transferred to a microcentrifuge tube. The tube was centrifuged, and the supernatant was discarded. Cytoplasmic extraction reagents were added to the cell pellet to lyse the cells, and the cytosolic supernatants were collected. Subsequently, nuclear extraction reagents were added to the cell pellets to extract nuclear proteins. The subsequent operations for protein analysis were consistent with standard WB procedures. The GAPDH and Lamin B1 were used as markers for the cytoplasmic and nuclear fractions, respectively.

Native Gel Electrophoresis to Separate the PKM2 Oligomer To analyze the oligomeric status of PKM2, protein samples were separated under non-denaturing conditions using native polyacrylamide gel electrophoresis (Native-PAGE). Briefly, total protein was extracted from HRMECs and quantified. After pretreatment with 5× loading buffer (P0016N, Beyotime, China), 20 μg of protein was separated using a Native-PAGE Gel Quick Preparation kit (MA0172, Mei Lun, China), transferred to a PVDF membrane and processed for standard WB.

Statistical Analysis Statistical analysis were performed using SPSS 26.0 and GraphPad Prism 10.0 (GraphPad, USA). Data are reported as mean±standard deviation (SD) from at least three independent experiments. Intergroup differences were assessed by Student's *t*-test (two groups) or one-way analysis of variance (ANOVA) with Brown-Forsythe and Welch tests (multiple groups), considering $P<0.05$ as statistically significant.

RESULTS

High Glucose Induces Pro-angiogenic Activation of HRMECs To evaluate the effects of HG on HRMEC function, we first examined the impact of HG treatment on cell proliferation at different time points. HG treatment consistently enhanced HRMEC proliferation from 24 to 72h, peaking at 48h of exposure (Figure 1A). Further EdU assay results revealed that 48h of HG treatment enhanced the proliferation capacity of HRMECs (Figure 1B). Tube formation assay results were consistent with these findings, showing a significant increase in the number of tubes after 48h of HG stimulation (Figure 1C). Scratch assay and migration assay analyses demonstrated that, compared to the control group, 48h of HG treatment significantly enhanced the migration ability of HRMECs (Figure 1D-1E). VEGFA and VEGFR2 are established regulators of endothelial cells vessel growth[26-27], we examined their involvement in HG-induced HRMEC activation. Quantitative RT-PCR analysis revealed that HG treatment significantly upregulated the mRNA levels of both VEGFA and VEGFR2 in HRMECs compared to the NG control (Figure 1F). WB analysis showed that HG treatment for 24 to 72h significantly promoted the expression of VEGFR2 and VEGFA (Figure 1G). All above results indicate that HG enhances the proliferation, migration, and tube-forming capacity of HRMECs.

PKM2 Knockdown Attenuates HG-induced Activation in HRMECs The functional role of PKM2 in HRMECs was investigated using a GFP-tagged lentiviral system. HRMECs were infected with lentivirus supernatant carrying either PKM2-specific shRNA or non-targeting shRNA (shNC). We first verified the infection efficiency through GFP fluorescence imaging (Figure 2A) and then evaluated the PKM2 knockdown efficiency by qRT-PCR and WB analysis for mRNA and protein expression, respectively (Figure 2B, 2C). To determine whether PKM2 influences HRMEC function under HG conditions, a series of functional assays were performed. The CCK-8 assay revealed that PKM2 knockdown significantly attenuated HRMEC viability under HG conditions (Figure 2D). EdU assay demonstrated that PKM2 silencing markedly inhibited HG-induced proliferation of HRMECs (Figure 2E). Transwell migration assays demonstrated a marked reduction in cell migration following PKM2 silencing in the HG environment (Figure 2F). Similarly, tube formation assays indicated that PKM2 knockdown considerably impaired the angiogenic capacity of HRMECs compared to the control group under HG stimulation (Figure 2G). To determine the impact on angiogenic signaling, we first assessed transcriptional changes. qRT-PCR analysis revealed that PKM2 silencing markedly reduced the HG-induced upregulation of VEGFA and VEGFR2 mRNA (Figure 2H). Consistently, WB analysis confirmed that PKM2 knockdown also suppressed the expression of these key pro-angiogenic factors at the protein level (Figure 2I). Collectively, these data identify PKM2 as a central node in HG-induced HRMEC activation.

HG Orchestrates PKM2 Phosphorylation, Dimerization, and Nuclear Translocation Functional experiments confirmed that PKM2 is essential for HG-induced HRMEC activation. Given that phosphorylation at Y105 is a critical regulator of PKM2 function, we focused on this modification, along with its oligomeric state and localization, to delineate the mechanisms of HG-induced PKM2 regulation. We first detected the phosphorylation level of PKM2 under HG conditions. Importantly, to rule out nonspecific effects of hyperosmolarity, we included an osmotic control using D-mannitol. HG treatment specifically induced the phosphorylation of PKM2 at Y105 in a time-dependent manner (peaking at 48h) in HRMECs, whereas mannitol treatment had no such effect (Figure 3A-3B). This result demonstrates that HG-induced PKM2 phosphorylation is a specific response to altered glucose metabolism, rather than a consequence of generalized hyperosmotic stress. Previous studies indicate

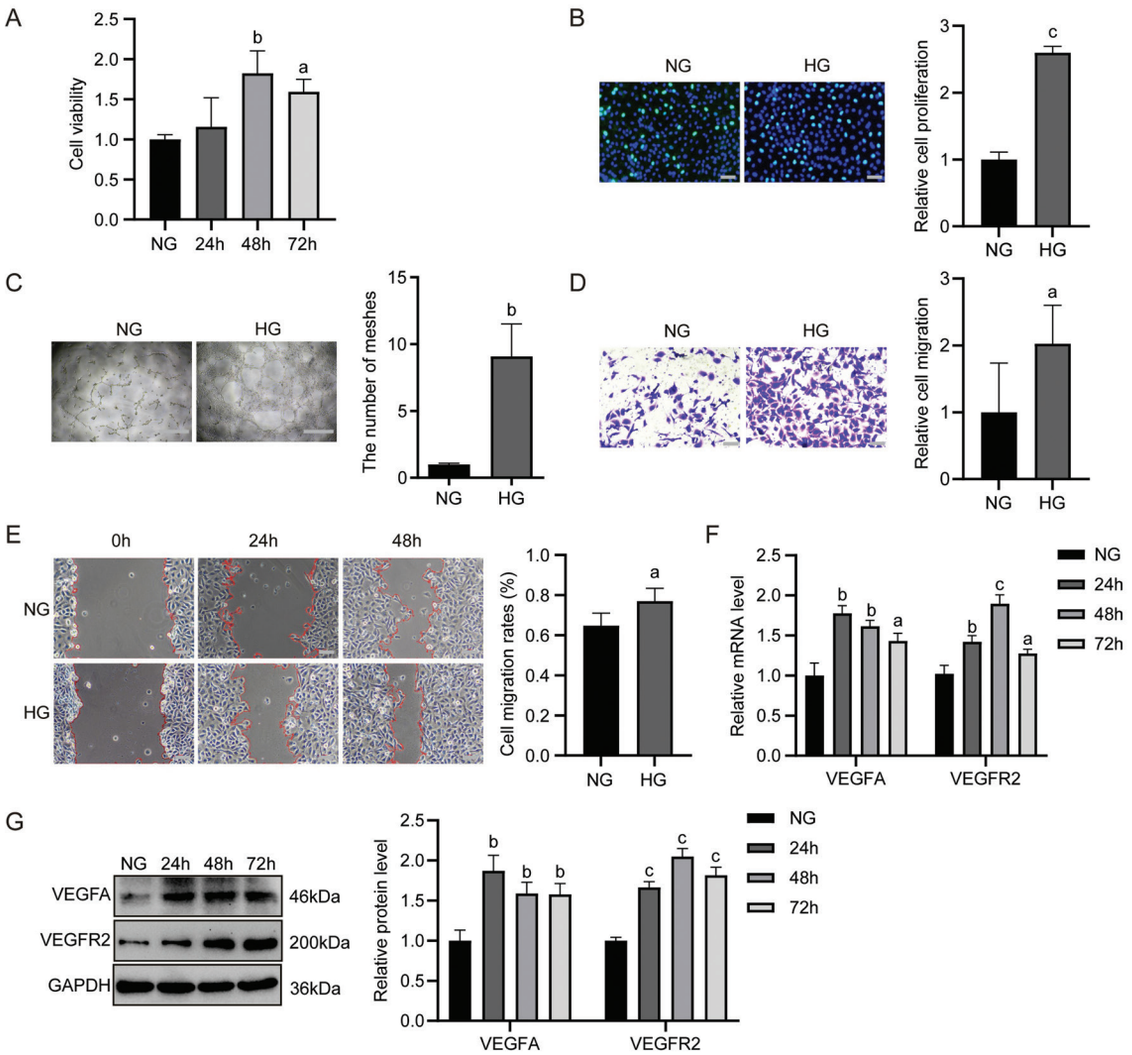

Figure 1 HG-induced the proliferation, migration, and angiogenesis in HRMECs A: Cell viability of HRMECs cultured with HG for the indicated time periods was measured by CCK-8 assay; B: Cell proliferation ability of HG treatment was measured by EdU assay (scale bar=100 μm); C: Tube formation of HRMECs was analyzed by Matrigel-based angiogenesis assay following HG exposure (scale bar=500 μm); D: Cell migration was evaluated using Transwell chambers of HG treatment (scale bar=100 μm); E: Cell migration was assessed by a scratch-wound assay. Representative images of HRMECs cultured under NG and HG conditions were captured after scratching (scale bar=100 μm); F: mRNA levels of VEGFA and VEGFR2 after HG treatment; G: Protein levels of VEGFR2 and VEGFA in HRMECs exposed to HG were detected by WB. All data are presented as mean±SD (n=3). [a]P<0.05, [b]P<0.01, [c]P<0.001 compared to the control group. All micrographs are representative of three biological replicates. HG: High glucose; HRMECs: Human retinal microvascular endothelial cells; CCK-8: Cell counting kit-8; EdU: 5-ethynyl-2'-deoxyuridine; NG: Normal glucose; VEGFA: Vascular endothelial growth factor A; VEGFR2: Vascular endothelial growth factor receptor 2; SD: Standard deviation; WB: Western blotting.

that the conformation and enzymatic activity of PKM2 are regulated by phosphorylation[28]. p-PKM2 (Y105) inhibits its tetramer formation and promotes the generation of dimers, a conformation associated with nuclear translocation and transcriptional co-regulatory functions[29]. To assess whether HG affects the oligomeric status of PKM2, we performed native gel electrophoresis. The results showed a significant decrease in the proportion of PKM2 tetramer in HG-treated HRMECs compared to the NG group (Figure 3C), indicating that HG promotes the transition of PKM2 from active tetramers to dimers. To determine whether dimeric PKM2 translocates to the nucleus to act as a transcriptional coactivator, we investigated its subcellular localization by nuclear-cytoplasmic fractionation and immunofluorescence. Both WB (Figure 3D) and immunofluorescence (Figure 3E) analyses consistently demonstrated a marked increase in PKM2 enrichment within the nucleus after 48h of HG stimulation. Analysis of subcellular fractions by native gel electrophoresis revealed that nuclear PKM2 exists predominantly as a dimer (Figure 3F). Our data support a model wherein HG induces PKM2 phosphorylation at Y105, promoting its tetramer-to-dimer shift and nuclear import to mediate non-metabolic functions in HRMECs.

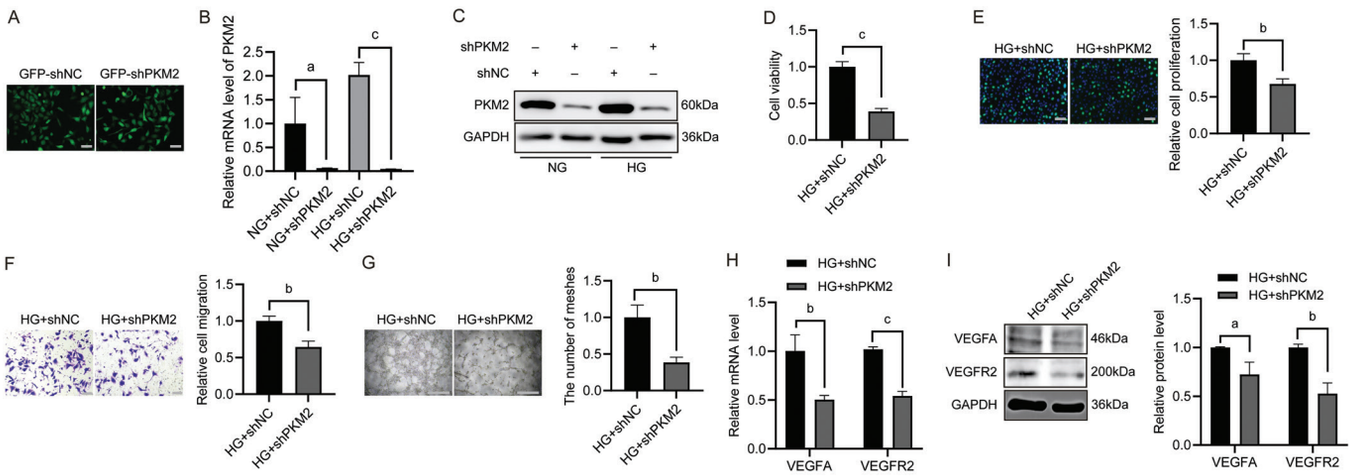

Figure 2 PKM2 knockdown attenuates HG-induced proliferation, migration, and angiogenesis in HRMECs HRMECs were infected with lentivirus expressing either non-targeting control shRNA (shNC) or PKM2-specific shRNA (shPKM2) to establish a PKM2 knockdown model, followed by culture under NG or HG conditions for 48h. A: The efficiency of infection was examined by GFP fluorescence (scale bar=100 μm); B, C: Knockdown efficiency was confirmed by WB and qPCR analysis after 48h; D: Cell viability was assessed by CCK-8 assay; E: Cell proliferation ability was measured by EdU assay (scale bar=100 μm); F: Cell migration was evaluated by Transwell assay (scale bar=100 μm); G: Angiogenic capacity was examined by tube formation assay (scale bar=500 μm); H: Transcriptional regulation of pro-angiogenic genes. mRNA levels of VEGFA and VEGFR2 were determined by qRT-PCR. Data were normalized to β-actin; I: Protein expression of pro-angiogenic factors. Protein levels of VEGFA and VEGFR2 were detected by WB and Densitometric quantification. All data are presented as mean±SD (n=3). [a]P<0.05, [b]P<0.01, [c]P<0.001 compared to the control group. All micrographs are representative of three biological replicates. PKM2: Pyruvate kinase M2; NG: Normal glucose; HG: High glucose; HRMECs: Human retinal microvascular endothelial cells; GFP: Green fluorescent protein; WB: Western blotting; qRT-PCR: Quantitative real-time polymerase chain reaction; CCK-8: Cell counting kit-8; EdU: 5-Ethynyl-2'-deoxyuridine; VEGFA: Vascular endothelial growth factor A; VEGFR2: Vascular endothelial growth factor receptor 2; SD: Standard deviation; GAPDH: Glyceraldehyde-3-phosphate dehydrogenase.

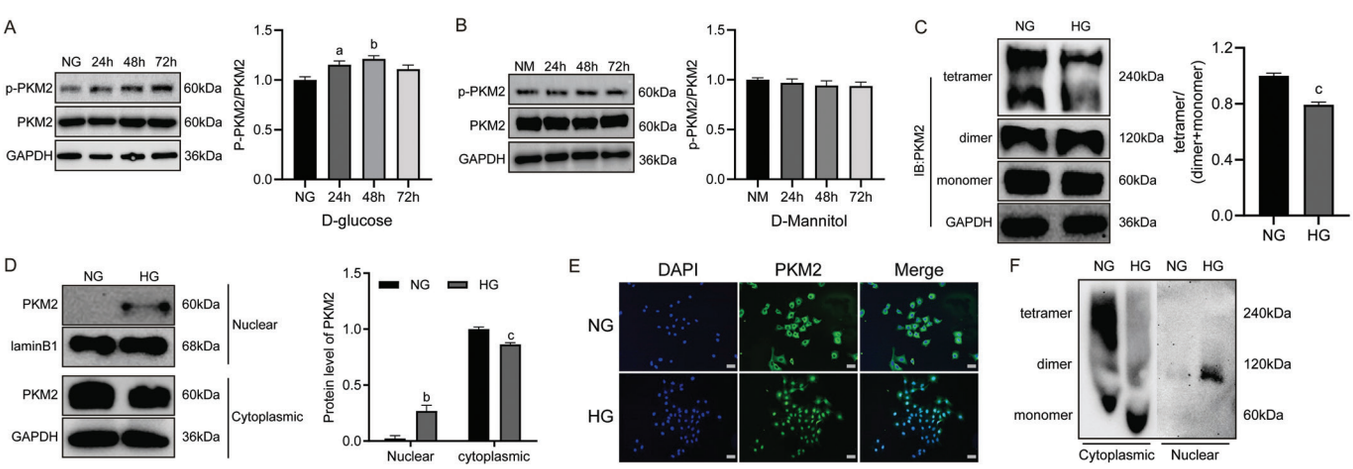

Figure 3 HG promotes PKM2 phosphorylation, dimerization, and nuclear translocation in HRMECs A: WB analysis of p-PKM2 (Y105) and total PKM2 expression in HG-induced HRMECs for the indicated time periods; B: WB analysis was performed to examine the levels of p-PKM2 (Y105) and total PKM2 in HRMECs treated with mannitol for the indicated time periods; C: Representative native gel electrophoresis blot showing the oligomeric status (tetramer and dimer/monomer) of PKM2 in HRMECs cultured under NG or HG conditions; D: Subcellular localization of PKM2 assessed by nuclear and cytoplasmic fractionation followed by WB. GAPDH and Lamin B1 were used as cytoplasmic and nuclear markers, respectively; E: Immunofluorescence staining of PKM2 (green) in HRMECs after 48h of HG exposure. Nuclei were visualized by DAPI (blue) staining (scale bar=100 μm); F: Native gel electrophoresis analysis of PKM2 oligomeric status in nuclear and cytoplasmic fractions extracted from HRMECs after 48h of HG treatment. All data are presented as mean±SD (n=3). [a]P<0.05, [b]P<0.01, [c]P<0.001 compared to the control group. All micrographs are representative of three biological replicates. HG: High glucose; HRMECs: Human retinal microvascular endothelial cells; WB: Western blotting; p-PKM2: Phosphorylated pyruvate kinase M2; Y105: Tyrosine 105; NG: Normal glucose; GAPDH: Glyceraldehyde-3-phosphate dehydrogenase; DAPI: 4',6-diamidino-2-phenylindole; SD: Standard deviation; IB: Immunoblotting.

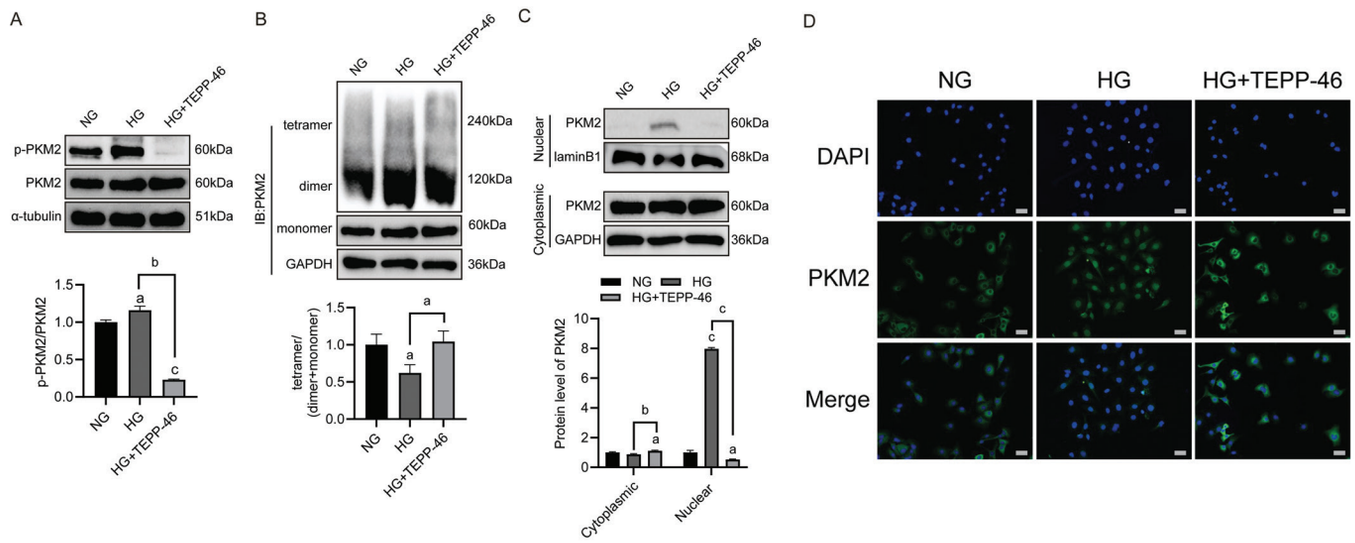

Figure 4 TEPP-46 suppresses HG-induced PKM2 activation and nuclear translocation HRMECs were cultured under NG, HG, or HG with TEPP-46 (10 μmol/L) for 48h. A: WB analysis of p-PKM2 (Y105) and total PKM2 protein levels; B: Native gel electrophoresis was used to assess the oligomeric status of PKM2; C: PKM2 subcellular localization was assessed by WB after cellular fractionation, using GAPDH and Lamin B1 to monitor cytoplasmic and nuclear fractions; D: Immunofluorescence staining of PKM2 (green) in HRMECs. Nuclei were visualized by DAPI (blue) staining (scale bar=100 μm). All data are presented as mean±SD (n=3). ^{a}P<0.05, ^{b}P<0.01, ^{c}P<0.001 compared to the control group. All micrographs are representative of three biological replicates. HG: High glucose; HRMECs: Human retinal microvascular endothelial cells; WB: Western blotting; p-PKM2: Phosphorylated pyruvate kinase M2; Y105: Tyrosine 105; NG: Normal glucose; GAPDH: Glyceraldehyde-3-phosphate dehydrogenase; DAPI: 4',6-diamidino-2-phenylindole; SD: Standard deviation; IB: Immunoblotting.

Pharmacological Stabilization of PKM2 Tetramers by TEPP-46 Attenuates HG-Induced PKM2 Activation Based on our findings that HG drives HRMEC activation *via* promoting PKM2 phosphorylation (Y105), dimerization, and nuclear translocation, we next investigated whether PKM2 conformational change is central to this process using the small-molecule activator TEPP-46. TEPP-46 specifically stabilizes the active tetrameric form of PKM2, consequently suppressing its dimerization and nuclear translocation[30-32]. We first verified the antagonistic effect of TEPP-46 on HG-induced PKM2 activation. WB analysis showed that co-treatment with TEPP-46 significantly reduced the level of p-PKM2 (Y105) compared to the HG group alone (Figure 4A). Native gel electrophoresis further confirmed that TEPP-46 treatment effectively reversed the HG-induced decrease in the PKM2 tetramer ratio and promoted tetramer formation (Figure 4B). Nuclear-cytoplasmic fractionation and immunofluorescence assays revealed that TEPP-46 markedly inhibited the HG-induced nuclear translocation of PKM2 (Figure 4C-4D), indicating its ability to retain PKM2 in the cytoplasm and restore its metabolic function. Collectively, these results demonstrate that TEPP-46 attenuates HG-induced PKM2 activation by promoting tetramerization, reducing phosphorylation at Y105, and suppressing nuclear translocation.

TEPP-46 Attenuates HG-Induced Proliferation, Migration, and Angiogenesis in HRMECs Following confirmation of the pharmacological efficacy of TEPP-46, we further evaluated its impact on HG-induced HRMEC functions. The CCK-8 assay demonstrated that TEPP-46 treatment significantly suppressed HG-promoted cell proliferation (Figure 5A). Both Transwell and scratch-wound assays indicated that TEPP-46 effectively attenuated HG-induced cell migration (Figure 5B-5C). Similarly, tube formation assays revealed a marked reduction in the angiogenic capacity of HRMECs under HG conditions upon TEPP-46 treatment (Figure 5D). To assess the effect at the transcriptional level, we first performed qRT-PCR analysis. TEPP-46 co-treatment effectively suppressed the HG-induced upregulation of mRNA for the key pro-angiogenic genes VEGFA and VEGFR2 (Figure 5E). Consistently, this transcriptional inhibition was mirrored at the protein level, as WB analysis confirmed that TEPP-46 reversed the HG-induced increase in VEGFA and VEGFR2 protein expression (Figure 5F). These results indicate that pharmacological stabilization of the PKM2 tetrameric conformation effectively inhibits HG-induced nuclear translocation of PKM2 and its downstream pro-angiogenic effects.

HG-induced Angiogenesis of HRMECs Through PKM2/HIF-1α Axis Having established that HG promotes PKM2 nuclear translocation, we next sought to identify its key transcriptional partners mediating pro-angiogenic effects. Based on HIF-1α's established role in DR and its known interaction with PKM2[33-35], we hypothesized that the PKM2/

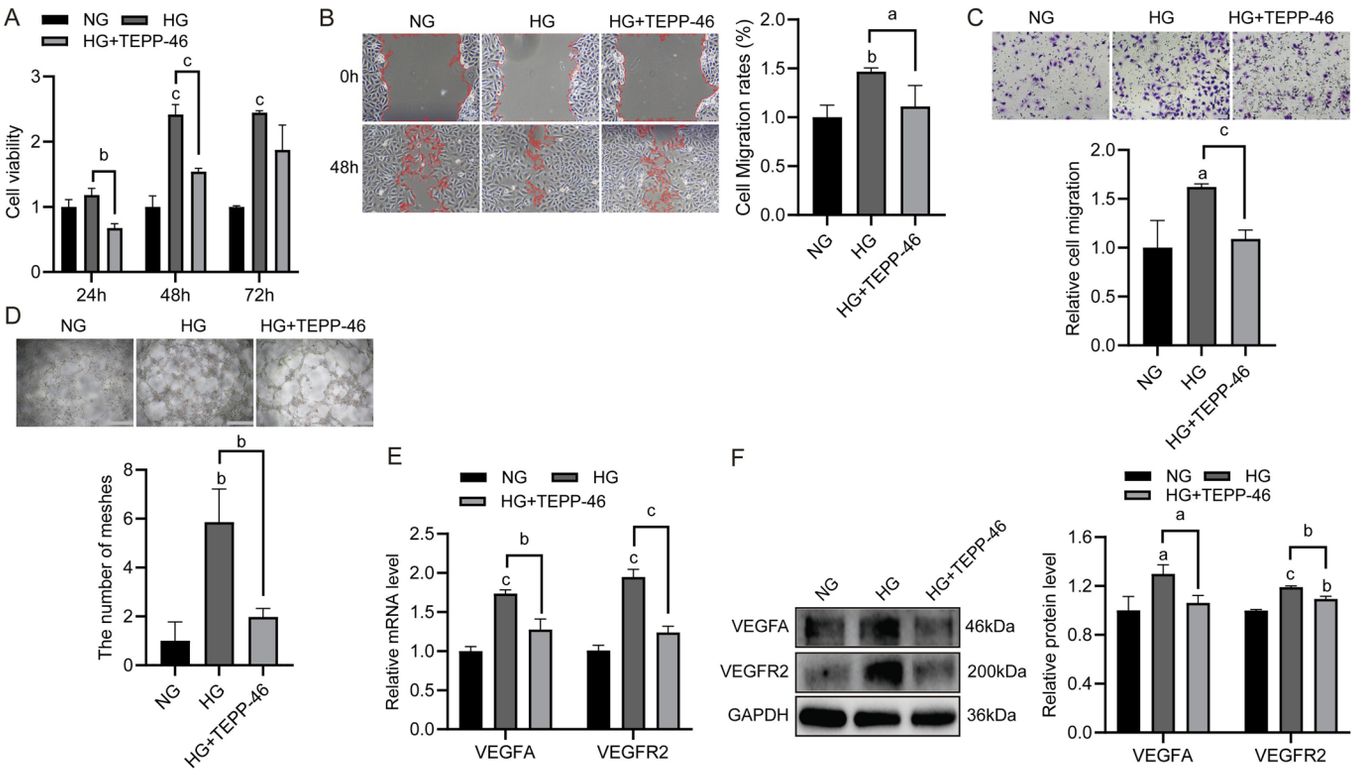

Figure 5 TEPP-46 attenuates HG-induced proliferation, migration, and angiogenesis in HRMECs HRMECs were exposed to NG, HG, and HG with TEPP-46 (10 μmol/L) for 48h. A: Cell viability was assessed by CCK-8 assay; B: Cell migration was evaluated by scratch-wound healing assay (scale bar=100 μm); C: Cell migration was further analyzed using Transwell chambers (scale bar=100 μm); D: Angiogenic capacity was examined by tube formation assay on Matrigel (scale bar=500 μm); E: Transcriptional regulation of pro-angiogenic genes. mRNA levels of VEGFA and VEGFR2 were determined by qRT-PCR. Data were normalized to β-actin; F: Protein expression levels and quantitative analysis protein levels of VEGFA and VEGFR2 were detected by WB. All data are presented as mean±SD (n=3). [a]P<0.05, [b]P<0.01, [c]P<0.001 compared to the control group. All micrographs are representative of three biological replicates. HG: High glucose; HRMECs: Human retinal microvascular endothelial cells; NG: Normal glucose; CCK-8: Cell counting kit-8; qRT-PCR: Quantitative real-time polymerase chain reaction; VEGFA: Vascular endothelial growth factor A; VEGFR2: Vascular endothelial growth factor receptor 2; WB: Western blotting; SD: Standard deviation.

HIF-1α axis plays a key role in HG-induced angiogenesis. Initially, we confirmed that HG treatment time-dependently upregulated HIF-1α protein expression in HRMECs (Figure 6A). Immunofluorescence analysis demonstrated notable nuclear translocation of both PKM2 and HIF-1α following HG exposure, with clear co-localization observed in the nucleus (Figure 6B), suggesting a potential interaction. To test this directly, we performed co-immunoprecipitation (Co-IP) assays using nuclear extracts. PKM2 specifically co-precipitated with HIF-1α under HG conditions, confirming a direct physical interaction within the nuclear compartment (Figure 6C). We next investigated whether PKM2 regulates HIF-1α signaling. WB analysis showed that PKM2 silencing significantly attenuated HG-induced HIF-1α protein expression (Figure 6D). Furthermore, qPCR analysis revealed that PKM2 knockdown specifically reduced HG-induced VEGFA mRNA levels without affecting HIF-1α transcription (Figure 6E-6F), indicating that PKM2 acts downstream of HIF-1α to regulate its target genes. Consistent with this, treatment with the PKM2 activator TEPP-46, which promotes tetramerization, effectively suppressed HG-induced upregulation of HIF-1α protein expression (Figure 6G). Collectively, these outcomes suggested that HG enhanced the PKM2 nuclear translocate and the interaction with HIF-1α, thereby amplifying VEGFA-mediated angiogenic signaling in HRMECs.

DISCUSSION

Our study unveils a novel mechanism whereby HG drives retinal angiogenesis by reprogramming the functional state of PKM2 in HRMECs. We demonstrate that HG induces a conformational switch in PKM2, shifting it from a tetrameric glycolytic enzyme to a dimeric form that translocates to the nucleus and exerts non-metabolic functions. Crucially, this conformational change is not merely correlative but essential for HG-induced angiogenic activation, as evidenced by both genetic knockdown and pharmacological stabilization of the tetrameric form.

A key finding of our work is the central role of PKM2's nuclear, non-metabolic function. While PKM2-mediated glycolytic ATP production supports endothelial cell anabolism[13-14], our data suggest that its pro-angiogenic effect in DR primarily relies on

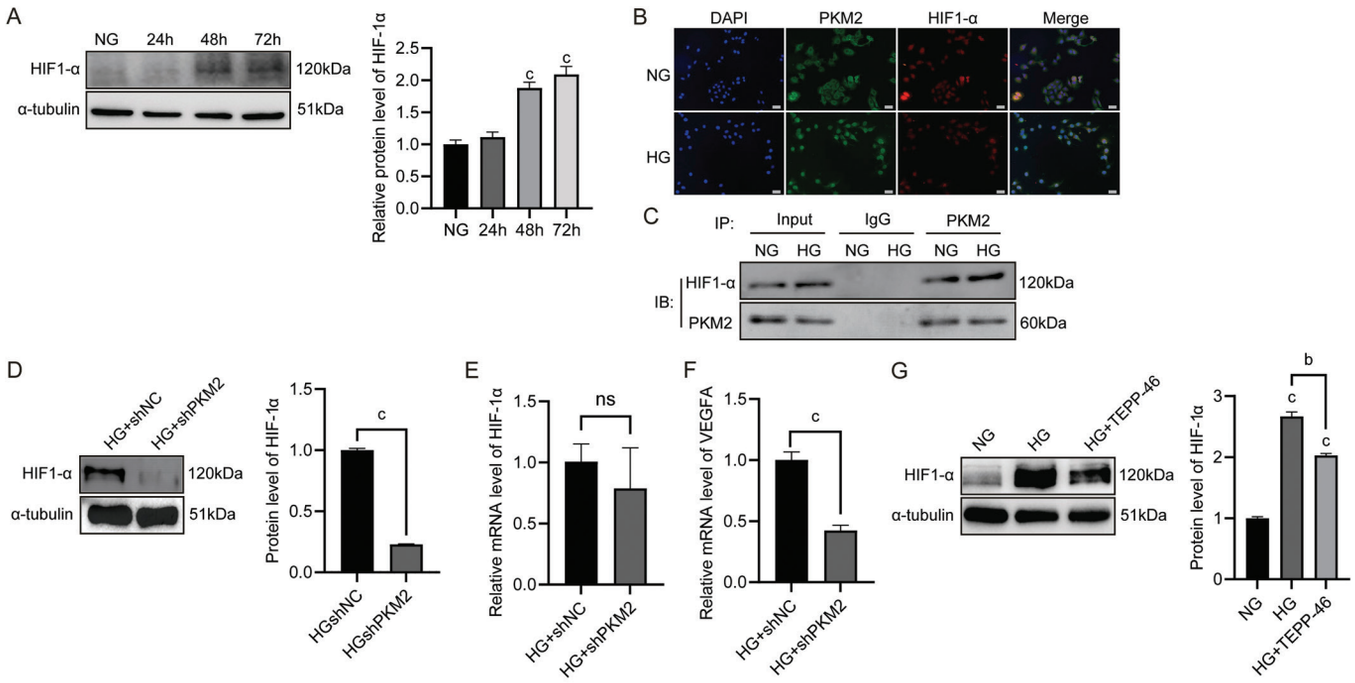

Figure 6 HG-induced angiogenesis of HRMECs through PKM2/HIF-1α axis A: HIF-1α expression in HRMECs exposure to HG for the indicated time periods, assessed by WB; B: Representative images of double immunofluorescence showing subcellular localization of PKM2 (green) and HIF-1α (red) in HRMECs cultured under NG or HG conditions. Nuclei were visualized by DAPI (blue) staining (scale bar=100 μm); C: Co-IP analysis of the interaction between PKM2 and HIF-1α. Nuclear extracts from HRMECs treated with NG or HG for 48h were immunoprecipitated with an antibody against PKM2 or control IgG. The immunoprecipitates and input lysates (5%) were immunoblotted with the indicated antibodies; D: WB analysis of HIF-1α expression in HRMECs infected with non-targeting control shRNA or PKM2-specific shRNA for 6h, followed by HG treatment for 48h; E, F: mRNA levels of HIF-1α and VEGFA in HRMECs treated as in (C), determined by qRT-PCR; G: WB analysis of HIF-1α expression in HRMECs treated with NG, HG, and HG with TEPP-46 (10 μmol/L) for 48h. All data are presented as mean±SD (n=3). ^{b}P<0.01, ^{c}P<0.001 compared to the control group. All micrographs are representative of three biological replicates. HG: High glucose; HRMECs: Human retinal microvascular endothelial cells; PKM2: Pyruvate kinase M2; HIF-1α: Hypoxia-inducible factor 1 alpha; WB: Western blotting; NG: Normal glucose; DAPI: 4',6-diamidino-2-phenylindole; Co-IP: Co-immunoprecipitation; IP: Immunoprecipitation; IgG: Immunoglobulin G; IB: Immunoblotting; qRT-PCR: Quantitative real-time polymerase chain reaction; VEGFA: Vascular endothelial growth factor A; SD: Standard deviation.

its nuclear role. This is strongly supported by the observation that TEPP-46, which promotes PKM2 tetramerization and cytosolic retention, effectively suppressed angiogenesis without compromising overall glycolytic flux. This paradigm—from metabolic enzyme to nuclear transcriptional co-regulator—aligns with its documented role in cancer[36-37] and highlights a targetable pathogenic mechanism in DR that is distinct from its metabolic function.

Further elucidating the nuclear mechanism, we identified the PKM2/HIF-1α axis as a critical signaling node. Our results position nuclear PKM2 as a key co-activator for HIF-1α, enhancing the expression of its target gene, VEGFA, under HG conditions. This is consistent with the established feed-forward loop between PKM2 and HIF-1α in cancer[33,38] and confirms its relevance in diabetic microvascular complications. The fact that PKM2 knockdown or TEPP-46 treatment attenuated HIF-1α protein levels and its downstream signaling without affecting HIF1A mRNA transcription suggests a post-translational regulatory mechanism, potentially involving stabilization or enhanced transactivation, which warrants further investigation.

Our study delineates a pathway wherein HG promotes PKM2 phosphorylation, nuclear translocation, and interaction with HIF-1α to drive angiogenesis in retinal endothelial cells. While our *in vitro* findings are supported by genetic and pharmacological evidence, several avenues for future validation and mechanistic deepening should be noted. First, the pathophysiological relevance of this axis requires confirmation in more complex systems. Future studies utilizing tissue-specific PKM2 knockout models or established diabetic animal models will be crucial to validate this pathway *in vivo*. Second, while we have demonstrated the physical interaction between nuclear PKM2 and HIF-1α, establishing a direct causal link from this complex to transcriptional activation would strengthen our model. Future chromatin immunoprecipitation (ChIP) assays could directly map PKM2 occupancy at the promoters of HIF-1α target genes such as VEGFA and VEGFR2. Furthermore, genetic or

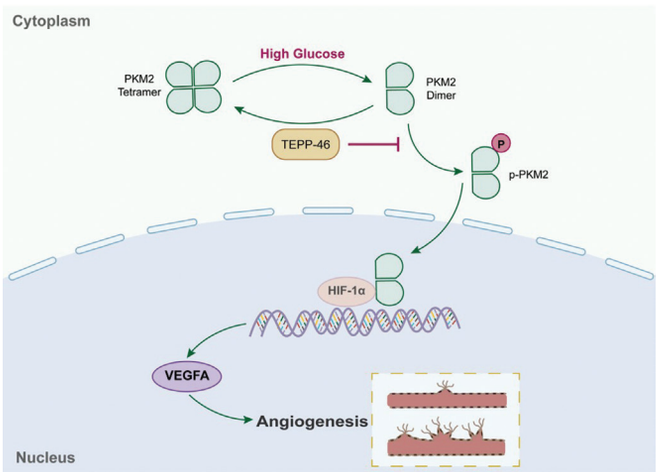

Figure 7 Proposed mechanism of PKM2 in HG-induced angiogenesis in HRMECs Under HG conditions, increased phosphorylation of PKM2 at Y105 promotes its transition from a tetrameric to a dimeric state and facilitates nuclear translocation. Nuclear PKM2 interacts with HIF-1α, enhancing its transcriptional activity and leading to upregulated VEGFA expression, thereby promoting angiogenesis. The small-molecule activator TEPP-46 stabilizes PKM2 in its tetrameric conformation, inhibiting dimerization, nuclear translocation, and subsequent HIF-1α/VEGFA-mediated angiogenic signaling. PKM2: Pyruvate kinase M2; HG: High glucose; HRMECs: Human retinal microvascular endothelial cells; Y105: Tyrosine 105; HIF-1α: Hypoxia-inducible factor 1 alpha; VEGFA: Vascular endothelial growth factor A.

pharmacological disruption of the PKM2-HIF-1α interaction, coupled with transcriptomic analysis, would help definitively attribute the pro-angiogenic gene program to this specific complex. Finally, to conclusively rule out potential off-target effects of our interventions, the most rigorous genetic approach would involve rescue experiments in which a nuclear-localized PKM2 mutant is re-expressed in a PKM2-knockdown background. Such experiments would unequivocally establish whether the angiogenic defects observed upon PKM2 depletion are specifically attributable to the loss of its nuclear function.

In conclusion, our findings propose a working model (Figure 7) for HG-induced angiogenesis in DR: HG promotes PKM2 phosphorylation at Y105, leading to its dimerization and nuclear translocation. Within the nucleus, PKM2 partners with HIF-1α to amplify the transcription of pro-angiogenic genes like VEGFA. Pharmacological stabilization of PKM2 in its tetrameric form by TEPP-46 disrupts this entire cascade. Therefore, targeting the conformational dynamics of PKM2 presents a promising therapeutic strategy for mitigating pathological neovascularization in DR.

ACKNOWLEDGEMENTS

Authors' Contributions: Liu TY, Tian YJ, Kuai PZ, Luo YS, Duan CW, Chen TP, and Wang XL conducted the experiments and data analysis; Liu TY, Tian YJ, and Cao X were involved in the experimental design and manuscript drafting; Zhang DM and Cao X revised the manuscript. All authors have read and approved the final version of this manuscript for publication.

Foundations: Supported by the National Natural Science Foundation of China [Young Scientists Program (No.82501314)]; Jiangsu Provincial Health Commission Scientific Research Project (No.M2024093); Natural Science Foundation (Youth Fund) of Science and Technology Bureau of Nantong City (No.JC2023028).

Conflicts of Interest: Liu TY, None; **Tian YJ,** None; **Kuai PZ,** None; **Luo YS,** None; **Duan CW,** None; **Chen TP,** None; **Wang XL,** None; **Zhang DM,** None; **Cao X,** None.

REFERENCES

1 LeDu JL, Ronco C. Therapeutic strategies targeting ocular vasculopathies: Current advances and emerging challenges. *Drug Discov Today* 2025;30(11):104496.

2 Li WQ, Zhang YR, Zhu HJ, *et al*. CAVIN3 deficiency promotes vascular normalization in ocular neovascular disease *via* ERK/JAG1 signaling pathway. *JCI Insight* 2025;10(9):e187836.

3 Liu L, Xu H, Zhao HY, *et al*. STEAP4 inhibits HIF-1α/PKM2 signaling and reduces high glucose-induced apoptosis of retinal vascular endothelial cells. *Diabetes Metab Syndr Obes Targets Ther* 2020;13:2573-2582.

4 Guo CY, Niu YQ, Pan XM, *et al*. Hypoglycemia promotes inner blood-retinal barrier breakdown and retinal vascular leakage in diabetic mice. *Sci Transl Med* 2025;17(796):eadq5355.

5 Tang K, Huang CC, Huang ZJ, *et al*. GPR30-driven fatty acid oxidation targeted by ginsenoside Rd maintains mitochondrial redox homeostasis to restore vascular barrier in diabetic retinopathy. *Cardiovasc Diabetol* 2025;24(1):121.

6 Boey E, Zaidi H, Tang TN, *et al*. Role of angiogenesis in retinal diseases and new advances in drug development. *Cells* 2025; 14(23):1849.

7 Kim D, Choi SW, Cho J, *et al*. Discovery of novel small-molecule antiangiogenesis agents to treat diabetic retinopathy. *J Med Chem* 2021;64(9):5535-5550.

8 Li XR, Sun XD, Carmeliet P. Hallmarks of endothelial cell metabolism in health and disease. *Cell Metab* 2019;30(3):414-433.

9 Guo Y, Yang R, Li Y, *et al*. Outcomes of anti-VEGF therapy compared with conventional interventions in diabetic retinopathy management. *Exp Ther Med* 2025;31(2):1-9.

10 Xu YN, Ma XH, Ni WY, *et al*. PKM2-driven lactate overproduction triggers endothelial-to-mesenchymal transition in ischemic flap *via* mediating TWIST1 lactylation. *Adv Sci* 2024;11(47):2406184.

11 Anastasakis DG, Apostolidi M, Garman KA, *et al*. Nuclear PKM2 binds pre-mRNA at folded G-quadruplexes and reveals their gene regulatory role. *Mol Cell* 2024;84(19):3775-3789.e6.

12 Rajala A, Soni K, Rajala RVS. Metabolic and non-metabolic roles of pyruvate kinase M2 isoform in diabetic retinopathy. *Sci Rep* 2020;10:7456.

13 Huang CY, Zhang DQ, Blecker C, *et al*. Effects of phosphoglycerate kinase 1 and pyruvate kinase M2 on metabolism and physiochemical changes in postmortem muscle. *Food Chem X* 2024;21:101125.

14 Toller-Kawahisa JE, Viacava PR, Palsson-McDermott EM, *et al*. Metabolic reprogramming of macrophages by PKM2 promotes IL-10 production *via* adenosine. *Cell Rep* 2025;44(1):115172.

15 Stone OA, El-Brolosy M, Wilhelm K, *et al*. Loss of pyruvate kinase M2 limits growth and triggers innate immune signaling in endothelial cells. *Nat Commun* 2018;9(1):4077.

16 Hu K, Xu JJ, Fan KR, *et al*. Nuclear accumulation of pyruvate kinase M2 promotes liver regeneration *via* activation of signal transducer and activator of transcription 3. *Life Sci* 2020;250:117561.

17 Zhang W, Zhang X, Huang S, *et al*. FOXM1D potentiates PKM2-mediated tumor glycolysis and angiogenesis. *Mol Oncol* 2021;15(5):1466-1485.

18 Li L, Tang L, Yang XP, *et al*. Gene regulatory effect of pyruvate kinase M2 is involved in RenalInflammation in type 2 diabetic nephropathy. *Exp Clin Endocrinol Diabetes* 2020;128(9):599-606.

19 Qi WE, Keenan HA, Li Q, *et al*. Pyruvate kinase M2 activation may protect against the progression of diabetic glomerular pathology and mitochondrial dysfunction. *Nat Med* 2017;23(6):753-762.

20 Luo WB, Hu HX, Chang R, *et al*. Pyruvate kinase M2 is a PHD3-stimulated coactivator for hypoxia-inducible factor 1. *Cell* 2011;145(5):732-744.

21 Wu HY, He LW, Shi JJ, *et al*. Resveratrol inhibits VEGF-induced angiogenesis in human endothelial cells associated with suppression of aerobic glycolysis *via* modulation of PKM2 nuclear translocation. *Clin Exp Pharma Physio* 2018;45(12):1265-1273.

22 Wang M, Wang Y, Xie TH, *et al*. Prostaglandin E2/EP2 receptor signalling pathway promotes diabetic retinopathy in a rat model of diabetes. *Diabetologia* 2019;62(2):335-348.

23 Li T, Han JB, Jia LJ, *et al*. PKM2 coordinates glycolysis with mitochondrial fusion and oxidative phosphorylation. *Protein Cell* 2019;10(8):583-594.

24 Yang P, Li ZW, Fu R, *et al*. Pyruvate kinase M2 facilitates colon cancer cell migration *via* the modulation of STAT3 signalling. *Cell Signal* 2014;26(9):1853-1862.

25 Zou J, Liu KC, Wang WP, *et al*. Circular RNA COL1A2 promotes angiogenesis *via* regulating miR-29b/VEGF axis in diabetic retinopathy. *Life Sci* 2020;256:117888.

26 Abhinand CS, Raju R, Soumya SJ, *et al*. VEGF-A/VEGFR2 signaling network in endothelial cells relevant to angiogenesis. *J Cell Commun Signal* 2016;10(4):347-354.

27 Li B, Zhang Y, Yin RT, *et al*. Activating CD137 signaling promotes sprouting angiogenesis *via* increased VEGFA secretion and the VEGFR2/Akt/eNOS pathway. *Mediat Inflamm* 2020;2020:1649453.

28 Alves-Filho JC, Pålsson-McDermott EM. Pyruvate kinase M2: a potential target for regulating inflammation. *Front Immunol* 2016;7:145.

29 Hitosugi T, Kang S, Vander Heiden MG, *et al*. Tyrosine phosphorylation inhibits PKM2 to promote the Warburg effect and tumor growth. *Sci Signal* 2009;2(97):ra73.

30 Lin MN, Huang LT, Huang JX, *et al*. Modulation of PKM2 inhibits follicular helper T cell differentiation and ameliorates inflammation in lupus-prone mice. *J Autoimmun* 2024;145:103198.

31 Liu HJ, Takagaki Y, Kumagai A, *et al*. The PKM2 activator TEPP-46 suppresses kidney fibrosis *via* inhibition of the EMT program and aberrant glycolysis associated with suppression of HIF-1α accumulation. *J Diabetes Invest* 2021;12(5):697-709.

32 Hasan DY, Gamen E, Abu Tarboush N, *et al*. PKM2 and HIF-1α regulation in prostate cancer cell lines. *PLoS One* 2018;13(9):e0203745.

33 Feng J, Wu LW, Ji J, *et al*. PKM2 is the target of proanthocyanidin B2 during the inhibition of hepatocellular carcinoma. *J Exp Clin Cancer Res* 2019;38(1):204.

34 Palsson-McDermott EM, Curtis AM, Goel G, *et al*. Pyruvate kinase M2 regulates hif-1α activity and IL-1β induction and is a critical determinant of the Warburg effect in LPS-activated macrophages. *Cell Metab* 2015;21(2):347.

35 Jiang J, Xia XB, Xu HZ, *et al*. Inhibition of retinal neovascularization by gene transfer of small interfering RNA targeting HIF-1α and VEGF. *J Cell Physiol* 2009;218(1):66-74.

36 Peng CF, Yang P, Zhang DS, *et al*. KHK-a promotes fructose-dependent colorectal cancer liver metastasis by facilitating the phosphorylation and translocation of PKM2. *Acta Pharm Sin B* 2024;14(7):2959-2976.

37 Zhang HY, Deng YH, Lu YT, *et al*. Differentiated T lymphocytes and cancer cell mitochondrial metabolism to enhance radioimmunotherapy by a biomimetic nanozyme system. *Adv Sci* 2026;13(3):e15097.

38 Zhang J, Ouyang F, Gao AB, *et al*. ESM1 enhances fatty acid synthesis and vascular mimicry in ovarian cancer by utilizing the PKM2-dependent Warburg effect within the hypoxic tumor microenvironment. *Mol Cancer* 2024;23(1):94.